Chapter 4

Liquid Crystal Wavefront Correctors

Li Xuan, Zhaoliang Cao, Quanquan Mu, Lifa Hu and Zenghui Peng

Additional information is available at the end of the chapter

http://dx.doi.org/10.5772/54265

1. Introduction

Liquid crystal (LC) was first discovered by the Austrian botanical physiologist Friedrich Reinitzer in 1888 [1]. It was a new state of matter beyond solid and liquid materials, having properties between those of a conventional liquid and those of a solid crystal. LC molecules usually have a stick shape. The average direction of molecular orientation is given by the director $\hat{n}$. When light propagates along the director $\hat{n}$, the refractive index is noted as the extraordinary index n_e, no matter the polarization direction (in the plane perpendicular to the long axis). However, the refractive index is different depending upon the polarization direction when light moves perpendicular to the director. When an electric field is employed, the LC molecule will be rotated so that the director $\hat{n}$ is parallel to the electric field. Due to the applied electric field, the LC molecular can be rotated from 0° to 90° and the effective refractive index is changed from n_e to n_o. As a result, the effective refractive index of LC can be controlled by controlling the strength of the electric field applied on the LC. The maximum change amplitude of the refractive index is birefringence $\triangle n = n_e - n_o$.

The properties discussed above allow LC to become a potential candidate for optical wavefront correction. A liquid crystal wavefront corrector (LCWFC) modulates the wavefront by the controllable effective refractive index, which is dependent on the electric field. As distinct from the traditional deformable mirrors, the LCWFC has the advantages of no mechanical motion, low cost, high spatial resolution, a short fabrication period, compactness and a low driving voltage. Therefore, many researchers have investigated LCWFCs to correct the distortions.

Initially, a piston-only correction method was used in LC adaptive optics (LC AOS) to correct the distortion. The maximum phase modulation equals $\triangle n$ multiplying the thickness of the LC layer, and it is about 1μm. As reported [2], the pixel size was over 1mm

and the number of pixels was about one hundred at that time. Because of the large pixel size, LCWFC not only loses the advantage of high spatial resolution but also mismatches the microlens array of the detector, which leads to additional spatial filtering in order to decrease the effect of the undetectable pixel for correction [3]. Moreover the small modulation amplitude makes it unavailable for many conditions. The thickness and Δn can be increased in order to increase the modulation amplitude. However, this will slow down the speed of the LCWFC.

Along with the development of LCWFC, an increasing number of commercial LC TVs are used directly for wavefront correction. Due to the high pixel density, the capacity for wavefront correction has been understood gradually by the researchers and the use of kinoform to increase the modulation amplitude is also possible [4-8]. A kinoform is a kind of early binary optical element which can be utilized in a high pixel density LCWFC. The wavefront distortion can be compressed into one wavelength with a 2π modulus of a large magnitude distortion wavefront. The modulated wavefront is quantified according to the pixel position of LCWFC. As discussed above, LCWFC only needs one wavelength intrinsic modulation amplitude to correct a highly distorted wavefront.

Many domestic and international researchers have devoted themselves to exploring LCWFCs from th 1970s onwards. In 1977, a LCWFC was used for beam shaping by I. N. Kompanets et al. [9]. S. T. Kowel et al. used a parallel alignment LC cell to fabricate a adaptive focal length plano-convex cylindrical lens in 1981 [10]. In 1984, he also realized a spherical lens by using two perpendicularly placed LC cells[11]. A LCWFC with 16 actuators was achieved in 1986 by A. A. Vasilev et al. and a one dimensional wavefront correction was realized [12]. Three years later, he realized beam adaptive shaping through 1296 actuators of an optical addressed LCWFC [13].

As a result, the LC AOS is becoming increasingly developed. In order to overcome the disadvantages of a traditional deformable mirror, such as a small number of actuators and high cost, D. Bonaccini et al. discussed the possibility of using LCWFC in a large aperture telescope [14, 15]. In 1995, D. Rensheng et al. used an Epson LC TV to perform a closed-loop adaptive correction experiment [16]. Although the twisted aligned LCWFC with the response time of 30ms was used, the feasibility of the LC AOS for wavefront correction was verified. Hence, many American [17-23], European [24-28] and Japanese [29] groups were devoted to the study of LC AOS. In 2002, the breakthrough for LC AOS was achieved and the International Space Station and various satellites were clearly observed [30]. In recent years, Prof. Xuan's group has completed series of valuable studies [31-42]. Recently, the applications of LCWFC have been extended to other fields, such as retina imaging [43-45], beam control [46-50], optical testing [41], optical tweezers [51-53], dynamic optical diffraction elements [54-57], tuneable photonic crystal fibre [58, 59], turbulence simulation [60, 61] and free space optical communications [62, 63].

The basic characteristics of a diffractive LCWFC are introduced in this chapter. The diffractive efficiency and the fitting error of the LCWFC are described first. For practical applications, the effects of tilt incidence and the chromatism on the LCWFC are

expounded. Finally, the fast response liquid crystal material is demonstrated as obtaining a high correction speed.

2. Diffraction efficiency

2.1. Theory

A Fresnel phase lens model is used to approximately calculate the diffraction efficiency of the LCWFC. According to the rotational symmetry and periodicity along the r^2 direction, when the Fresnel phase lens is illuminated with a plane wave of unit amplitude, the complex amplitude of the light can be expressed as [64]:

$$f(r^2) = f(r^2 + jr_p^2) \tag{1}$$

where j is an integer and the period isr_p^2. Also, it can be expressed by the Fourier series:

$$f(r^2) = \sum_{n=-\infty}^{+\infty} A_n \exp[i2\pi n r^2 / r_p^2] \tag{2}$$

The distribution of the complex amplitude at the diffraction order n can be obtained [65]:

$$A_n = 1/r_p^2 \int_0^{r_p^2} f(r^2) \exp[i2\pi n r^2 / r_p^2] dr^2 \tag{3}$$

For the Fresnel phase lens, the light is mainly concentrated on the first order (n=1). The diffraction efficiency of the Fresnel phase lens is defined as the intensity of the first order at its primary focus:

$$\eta = I(n=1) = |A_1|^2 \tag{4}$$

If the phase distribution function $f(r^2)$ of the Fresnel phase lens can be achieved, the diffraction efficiency can be calculated by Eq. (3) and Eq. (4).

To correct the distorted wavefront, the 2π modulus should be performed first to wrap the phase distribution into one wavelength. Then, the modulated wavefront will be quantized. For a example, the wrapped phase distribution of a Fresnel phase lens is shown in Fig. 1(a). To a Fresnel phase lens, the 2π phase is always quantized with equal intervals. Assuming the height before quantization is h, the quantization level is N and the height of each quantized step is h/N. Figure 1(b) is a Fresnel phase lens quantized with 8 levels.

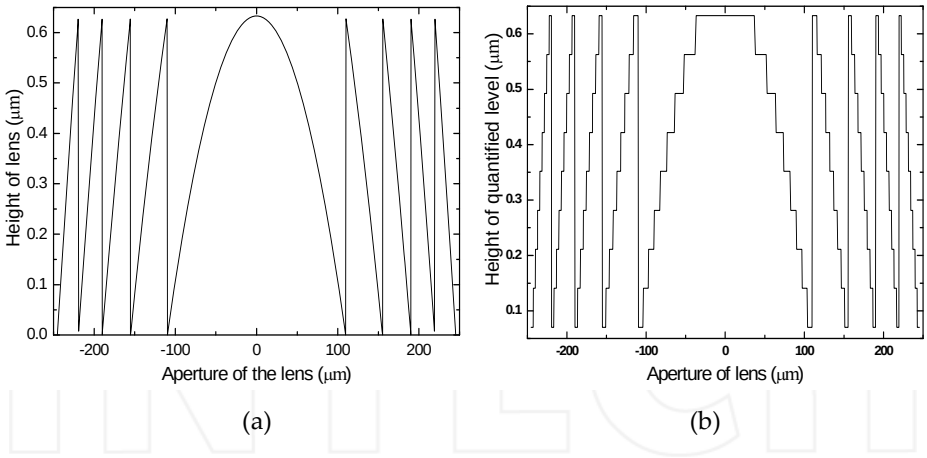

Figure 1. Phase distribution of a Fresnel phase lens: (a) 2π modulus; (b) quantized.

For a quantized Fresnel phase lens, the diffraction efficiency can be expressed as [66]:

$$\eta = \sin c^2\left(1/N\right) \tag{5}$$

Figure 2 shows the diffraction efficiency as a function of the quantization level for a Fresnel phase lens.

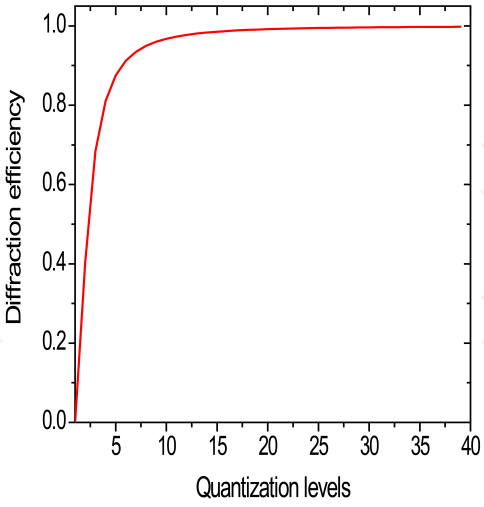

Figure 2. Diffraction efficiency as a function of the quantization level.

http://dx.doi.org/10.5772/54265

2.2. Effects of black matrix

A LCWFC always has a Black Matrix, which will cause a small interval between each pixel, as shown in Fig. 3. At the interval area, the liquid crystal molecule cannot be driven and then the phase modulation is different to the adjacent area. This will affect the diffraction efficiency of the LCWFC, as shown in Fig. 4. It is seen that the diffraction efficiency decreases by 6.4%, 8.8%, 9.5% and 9.7%, respectively for 4, 8, 16 and 32 levels, while the pixel interval is 1μm and the pixel pitch is 20μm. Consequently, the effect magnitude of the diffraction efficiency increases for a larger number quantified levels while the maximum decrease of the diffraction efficiency is about 10%.

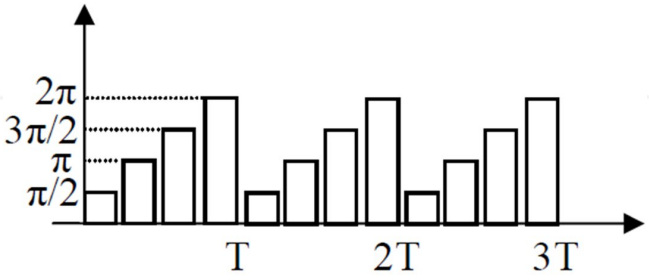

Figure 3. A Fresnel phase lens quantified by the pixel with a Black Matrix.

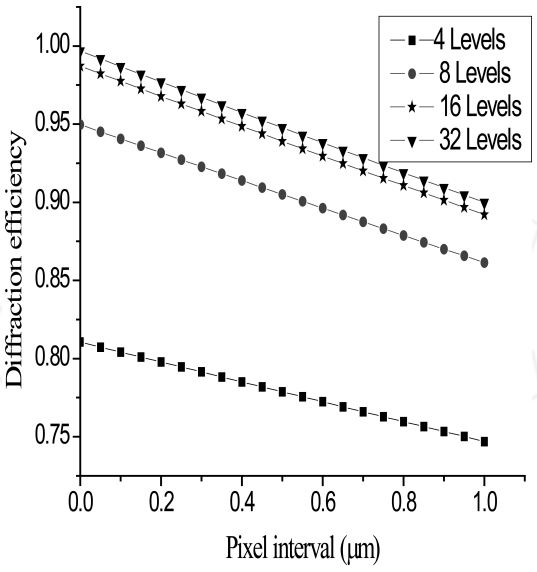

Figure 4. The diffraction efficiency as functions of the pixel interval for different quantified levels.

2.3. Mismatch between the pixel and the period

Because the pixel has a certain size P, the period T of a Fresnel phase lens cannot be divided exactly by the pixel, as shown in Fig. 5. This error is similar to the linewidth error caused by the lithography technique. For one period, the integer is n and the remainder is γ after T modulo P. If $\gamma \leq 0.5P$, there are n pixels in one period; on the contrary, there are n+1 pixels. As such, the maximum error is 0.5P for the first period. According to Eq. (3), the distribution of the complex amplitude of the first order can be acquired with the known phase distribution function in one period. Then, the diffraction efficiency can be obtained. As shown in Fig. 6, when the error of the first period changes from 0 to 0.5P, the diffraction efficiency decreases from 81% to 78.3%. The pixel number effect on the variation of the diffraction efficiency is also calculated while the error is 0.5P (Fig. 7). The decrease of the diffraction efficiency is 1% when the pixel number is 7. Accordingly, if the pixel number is not less than 7 in one period, the effect of the pixel size can be ignored.

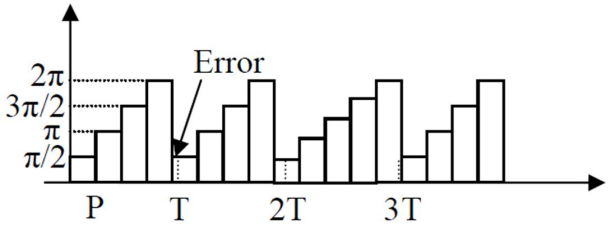

Figure 5. The mismatch between the pixel and the period of the Fresnel lens.

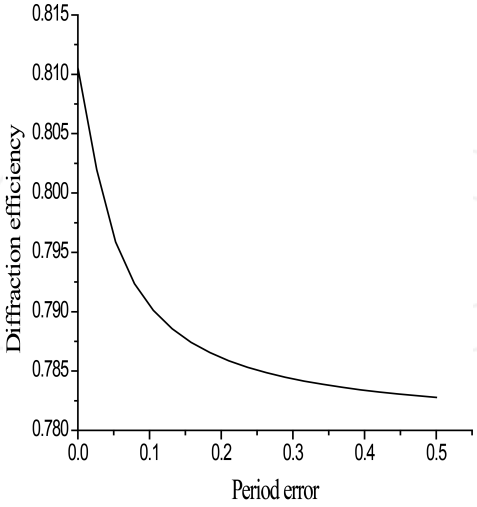

Figure 6. The diffraction efficiency as a function of the period error.

http://dx.doi.org/10.5772/54265

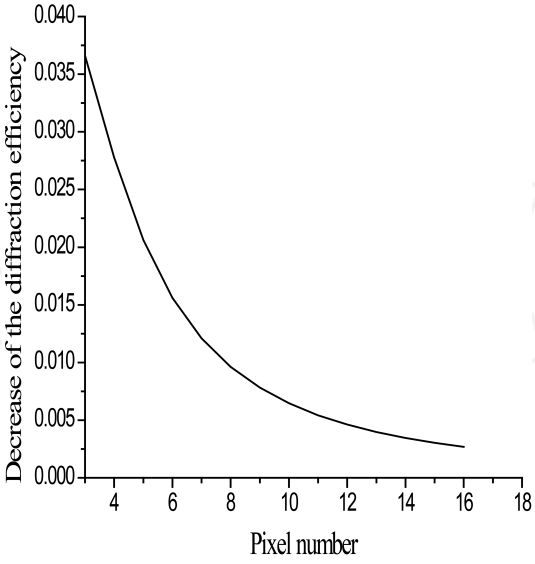

Figure 7. The decrease of the diffraction efficiency as a function of the pixel number.

2.3.1. Wavefront compensation error

The wavefront compensation error always exists due to the finite number of the wavefront correction element used for the correction of the atmospheric turbulence. Hudgin gave the relationship between the compensation error and the actuator size as follows [67]:

$$f = \alpha(\frac{r_s}{r_0})^{5/3} \tag{6}$$

where r_s is the actuator spacing, r_0 is the atmosphere coherence length and α is a constant depending on the response function of the actuator. For continuous surface deformable mirrors (DMs), the response function of the actuator is a Gaussian function and α ranges from 0.3-0.4 [68]. For a piston-only response function, α is 1.26 [69]. Researchers always use a piston-only response function to evaluate a LCWFC and have proved that the actuators need to be 4-5 times as large as that of the DM's [69, 70]. However, the case is totally different when a diffractive LCWFC (DLCWFC) is used where the kinoform or phase wrapping technique is employed to expand the correction capability [71, 72]. Therefore, Eq. (6) is not suitable any more.

2.4. The effect of quantization on the wavefront error

Firstly, the wavefront error generated during the phase wrapping due to quantization is considered. Since a LCWFC is a two-dimensional device, the quantification is performed along the x and y axes by taking the pixel as the unit. According to the diffraction theory, the correction precision as a function of the quantization level can be deduced [73]. If the pixel size is not considered, the root mean square (RMS) error of the diffracted wavefront as a function of the quantization level can be simplified as [73]:

$$\Delta W = \frac{\lambda}{2\sqrt{3}N} \tag{7}$$

Where N is the quantization level and λ is the wavelength. If N=30, then the RMS error can be as small as λ/100. For N=8, RMS=0.036λ and the corresponding Strehl ratio is 0.95. Figure 8 shows the diffracted wavefront RMS error as a function of the quantization level N. As can be seen, the wavefront RMS error reduces drastically at first, and then approaches to a constant gradually when the quantization level becomes greater than 10. The wavefront RMS error can be calculated for a known quantization level on a wavefront. For a DLCWFC, the wavefront compensation error is directly determined by the quantization level without any need to consider the pixel number. Therefore, the distribution of the quantization level on the atmospheric turbulence should be calculated first for a given pixel number, telescope aperture and atmospheric coherence length, and then the wavefront compensation error can be calculated by using Eq. (7).

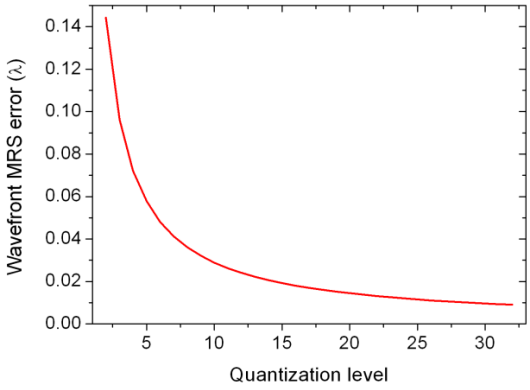

Figure 8. The wavefront RMS error as a function of the quantization level.

2.5. Zernike polynomials for atmospheric turbulence

Kolmogorov turbulence theory is employed to analyse the distribution of the quantization level across an atmospheric turbulence wavefront. Noll described Kolmogorov turbulence by using Zernike polynomials [74]. According to him, Zernike polynomials are redefined as:

$$\begin{aligned} Z_{even\ \ j} &= \sqrt{2(n+1)}R_n^m(\rho)\cos(m\theta),\ m \neq 0 \\ Z_{odd\ \ j} &= \sqrt{2(n+1)}R_n^m(\rho)\sin(m\theta),\ \ m \neq 0 \\ Z_j &= \sqrt{(n+1)}R_n^0(\rho), \qquad\qquad m=0 \end{aligned} \tag{8}$$

Where:

$$R_n^m(\rho) = \sum_{s=0}^{(n-m)/2} \frac{(-1)^s (n-s)!}{s!\left[\frac{(n+m)}{2}-s\right]!\left[\frac{(n-m)}{2}-s\right]!} \cdot r^{n-2s} \tag{9}$$

The parameters n and m are integral and have the relationship $m \leq n$ and $n - |m| = even$. An atmospheric turbulence wavefront can be described by using a Kolmogorov phase structure function, as below [74]:

$$D(r) = 6.88\left(\frac{r}{r_0}\right)^{5/3} \tag{10}$$

By combining the phase structure function and the Zernike polynomials, the covariance between the Zernike polynomials Z_j and $Z_{j'}$ with amplitudes a_j and $a_{j'}$ can be deduced as [75]:

$$\left\langle a_j a_{j'} \right\rangle = \begin{cases} \dfrac{K_{zz'}\delta_{mm'}\Gamma\left[(n+n'-5/3)/2\right](D/r_0)^{5/3}}{\Gamma\left[(n-n'+17/3)/2\right]\Gamma\left[(n'-n+17/3)/2\right]\Gamma\left[(n+n'+23/3)/2\right]} & j-j' = even \\ 0, & j-j' = odd \end{cases} \tag{11}$$

where $K_{zz'} = 2.698(-1)^{(n+n'-2m)/2}\sqrt{(n+1)(n'+1)}$ and D is the telescope diameter. $\delta_{mm'}$ is the Kronecker delta function. By using Eq. (11), the coefficients of the Zernike polynomials can be easily computed. If the first J modes of the Zernike polynomials are selected, the atmospheric turbulence wavefront is represented as:

$$\phi_t = \sum_{j=1}^{J} a_j Z_j \tag{12}$$

Therefore, the atmospheric turbulence wavefront Φ_t can be calculated by using Eqs. (11) and (12). As the phase wrapping technique is employed, the atmospheric turbulence wavefront can be wrapped into 2π and quantized and thus the distribution of the quantization level across a telescope aperture D can be determined.

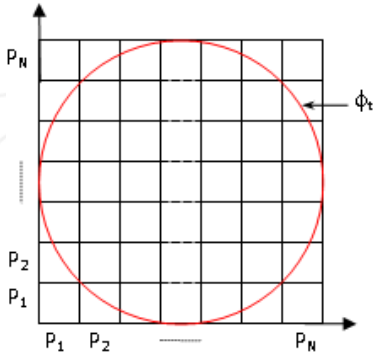

Figure 9. The field of the DLCWFC - the circle represents the wavefront of atmospheric turbulence and $P_1 \ldots P_N$ are the pixel numbers of the DLCWFC.

2.6. Calculation of the required pixel number of DLCWFCs

In practice, people hope to calculate the desired pixel number of a DLCWFC expediently for a given telescope aperture D, a quantization level N, and an atmospheric coherence length r_0. Therefore, it is necessary to deduce the relation between the pixel number of the DLCWFC and D, N and r_0. As shown in Fig. 9, the DLCWFC aperture can be represented by the pixel number across the aperture, which is called P_N. The circle represents the atmospheric turbulence wavefront Φ_t. Since the atmospheric turbulence wavefront is random, the ensemble average $\langle\Phi_t\rangle$ should be used in the calculation. The modulated and quantized atmospheric turbulence wavefront can be expressed as:

$$\mathrm{mod}(\langle\phi_t\rangle) = f(N, D, r_0, \langle P_N\rangle) \tag{13}$$

where mod( ) denotes the modulo 2π. If $\langle\Phi_t\rangle$ is known, $\langle P_N\rangle$ can be expressed as a function of the telescope aperture D, the quantization level N, and the atmospheric coherence length r_0. By using Eqs. (11) and (12), $\langle\Phi_t\rangle$ can be calculated and the first 136 modes of the Zernike polynomials are used in the calculation. For the randomness of the atmospheric turbulence wavefront, different quantization levels are used during the quantization, depending upon the fluctuation degree of the wavefront. Here, N is defined as the minimum quantization level so that the sum of those quantization levels greater than N should occupy 95% of the quantization levels included in the atmospheric turbulence wavefront. Fifty atmospheric turbulence wavefronts are used to achieve the statistical results. First, the relation between

http://dx.doi.org/10.5772/54265

the pixel number P_N and the telescope aperture D is calculated for r_0=10cm and N=16, as shown in Fig. 10. It can be seen that $<P_N>$ is a linear function of D when N and r_0 are fixed. That is to say, the larger the aperture of the telescope, the more the pixel number will be needed if a DLCWFC is used to correct the atmospheric turbulence. Specifically, for a telescope with a diameter of 2 metres, the total pixel number will be 96×96, while for a telescope with a diameter of 4 metres the total pixel number will be 168×168. P_N as a function of N is also computed for r_0=10cm and D =2 m, as shown in Fig.11. It illustrates that when D and r_0 are fixed, $<P_N>$ is a linear function of N. This means that the more that the quantization level is used, the more the pixel number will be needed.

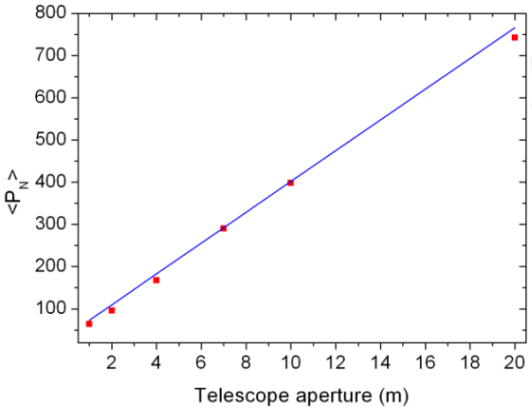

Figure 10. as a function of the telescope aperture D - ■ represents the calculated data for r_0=10 cm and N=16, and the solid curve represents the fitted data.

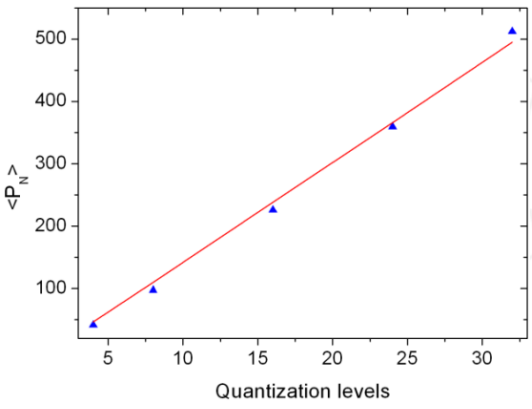

Figure 11. as a function of the quantization level N - ▲ represents the calculated data for D=2 m and r_0=10 cm, and the solid curve represents the fitted data.

The relationship between $\langle P_N \rangle$ and r_0 is also calculated with the variables N and D. Figure 12 shows only three curves with three pairs of fixed N and D. This time, the relationship is not a linear function anymore but an exponential function. With more pairs of N and D fixed, more curves can be obtained, but these are not shown in the figure. The relationship between $\langle P_N \rangle$ and r_0 can be expressed by the following formula:

$$\langle P_N \rangle = A + Br_0^{-6/5} \tag{14}$$

where A and B are the coefficients. A is only related to N and can be expressed as A=6.25N. As $\langle P_N \rangle$ is a linear function of D and N, the coefficient B can be expressed as:

$$B = a + bN + cD + dND \tag{15}$$

where a, b, c and d are the coefficients. By substituting the known value of N, D and the calculated coefficient B, the value of a, b, c and d is determined to be 15, -23, -150 and 91, respectively, by using the least-square method. Thus, $\langle P_N \rangle$ can be expressed as:

$$\langle P_N \rangle = 6.25N + \left(15 - 1.5D - 23N + 0.91ND\right) r_0^{-6/5} \tag{16}$$

where the units of D and r_0 is centimetres. The total pixel number of the DLCWFC can be calculated by using $P_N \times P_N$. By combining Eqs. (7) and (16), the compensation error of the DLCWFC can be evaluated for the atmospheric turbulence correction. These two formulas are not suitable for modal types of LCWFCs [76] or other types that do not use the diffraction method to correct the atmospheric turbulence.

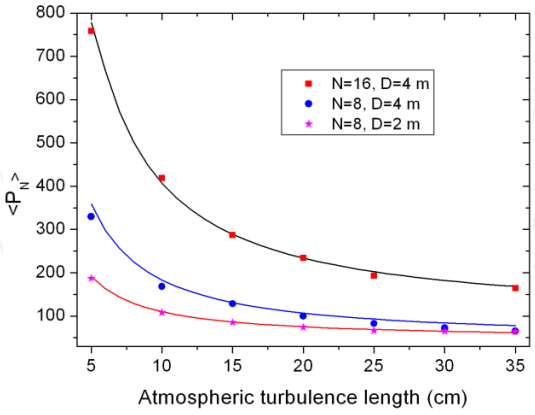

Figure 12. as a function of the atmosphere coherence length r_0 - the line is the fitted curve and ■, ● and ∗ represent the computed data with N=16 and D=4 m, N=8 and D=4 m, and N=8 and D=2 m, respectively.

http://dx.doi.org/10.5772/54265

Normally, the quantization level of 8 is suitable for the atmospheric turbulence correction for three reasons. Firstly, a higher correction accuracy can be obtained. When N=8, the RMS error can be reduced down to 0.035λ and the Strehl ratio can be increased to 95%. Secondly, a higher diffraction efficiency can be obtained. According to the diffractive optics theory [73], the diffraction efficiency is as large as 95% for N=8. Finally, the total pixel number can be controlled within a reasonable range. Of course, a smaller wavefront RMS error and a higher diffraction efficiency can be achieved with a larger quantization level. But, in that case, the required pixel number of the DLCWFC will be increased drastically, which will lead to a significantly slower computation and data transformation rate of the LCAOS. Fig. 13 shows the relation between P_N, D and r_0 for N=8. As can be seen, the desired pixel number apparently increases when the atmospheric coherence length becomes smaller and the telescope aperture becomes larger. For instance, the total pixel number of the DLCWFC is 1700×1700 when r_0=5 cm and D=20 m. However, if r_0=10 cm, the total pixel number can be reduced down to 768×768. Therefore, the strength of the atmosphere turbulence is a key factor which must be considered when designing the LCAOS for a ground-based telescope.

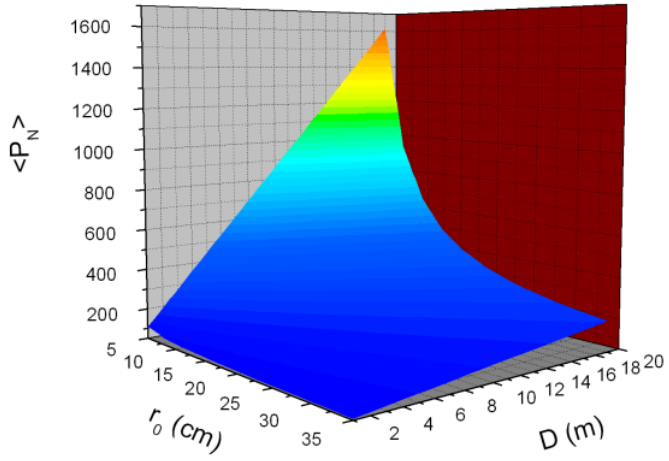

Figure 13. as functions of the atmosphere coherence length r_0 and the telescope aperture D for N=8.

2.6.1. Tilt incidence

Currently, reflective LCWFC devices [77-79], such as liquid crystal on silicon (LCOS) devices, are especially attractive because of their small fill factor, high reflectivity and short response time. To separate the incident beam from the reflected beam for a reflective LCWFC, the incident light should go to the LCWFC with a tilt angle. Alternatively, the

incident light is perpendicular to the LCWFC and a beam splitter is placed before the LCWFC to separate the reflected and incident beams. However, the second method will result in a 50% loss in each direction, reducing output power to 25% of the input. To avoid the energy loss, the tilt incidence is a suitable method for a LCWFC. However, the tilt incidence will affect the phase modulation and the diffraction efficiency of the LCWFC. A reflective LCWFC model is selected to perform the analysis and the acquired results are suitable for the transmitted LCWFC.

2.7. Effect of the tilt incidence on the phase modulation of the LCWFC

In order to simplify the model of the reflective LCWFC, the border effect is neglected and all of the molecules have the same tilt angle. The simplified model is shown in Fig.14. The former board is glass and the back is silicon. The liquid crystal molecule is aligned parallel to the board. The tilt incident angle is θ′. The liquid crystal material is a uniaxial birefringence material - it has an ordinary index n_o and the extraordinary index $n_e(\theta)$. $n_e(\theta)$ can be obtained with the index ellipsoid equation [41]:

$$n_{\mathrm{e}}(\theta)=\frac{n_{\mathrm{o}}n_{\mathrm{e}}}{\left(n_{\mathrm{o}}{}^{2}\cos^{2}\theta+n_{\mathrm{e}}{}^{2}\sin^{2}\theta\right)^{1/2}}, \tag{17}$$

where θ represents the tilt angle of the molecule and n_e is the off-state extraordinary refractive index. Assume that the LCWFC without the applied voltages and the polarization direction is the same as the LC director. For the tilt incidence as shown in Fig.14, it is equivalent to the rotation of the LC director with an angle θ'. Hence, although the tilt angle of the molecule is zero, the extraordinary refractive index is changed to $n_e(\theta')$ with the tilt incidence. Furthermore, the tilt incidence will change the transmission distance of the light in the liquid crystal cell with a factor of $1/\cos\theta'$. Consequently, the phase modulation with the tilt incidence and no applied voltages can be expressed as:

$$P_{tilt}=\frac{2\pi(n_e(\theta')-n_o)d}{\lambda\cos\theta'}. \tag{18}$$

If the pre-tilt angle of the liquid crystal molecule is considered, Eq.(18) can be rewritten as:

$$P_{tilt}=\frac{2\pi(n_e(\theta'+\theta_0)-n_o)d}{\lambda\cos\theta'}, \tag{19}$$

where θ_0 is the pre-tilt angle, d is the thickness of the liquid crystal cell and λ is the relevant wavelength.

http://dx.doi.org/10.5772/54265

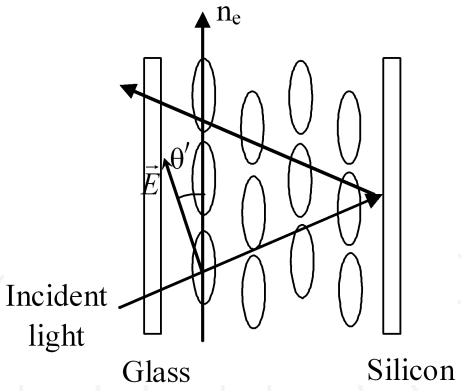

Figure 14. Simplified model of the reflective LCWFC with tilt incidence.

For n_e=1.714, n_o=1.516, λ=633nm and d=1.6μm, the phase modulation as a function of the incident angle is shown in Fig.15. The simulated results show that the phase modulation is reduced by at most 1% for incident angles under 6°. The measured result is also shown in the figure. The trends of the simulated and measured curves are similar. The difference of in phase shift might be caused by the border effect. For the actual liquid crystal cell, a rubbing polyimide (PI) film is used to align the liquid crystal molecules. The PI layer will anchor the liquid crystal molecules at the border; this causes the tilt angle of the liquid crystal molecule at the interface to be different from the centre. The simulated and measured results indicate that the LCWFC may be used with a small tilt angle.

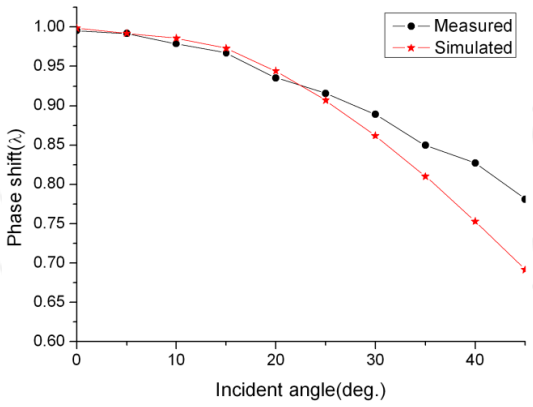

Figure 15. Phase shift as a function of the incident angle - -●- is the measured curve and -∗- represents the simulated data.

2.8. The effect of pixel crossover on the phase modulation

For the tilt incidence, shown in Fig.16, the incident light in one pixel could transmit through an adjacent pixel, which is called pixel crossover. The maximum error of the pixel crossover is *W*. The pixel crossover will also affect the phase modulation of the LCWFC. Because each pixel is an actuator with a corresponding phase modulation, the light should go through just one pixel so as to control the phase modulation accurately. For a 19μm pixel size and *d*=1.6μm, *W* as a function of the incident angle is shown in Fig.17. The results show that *W*=0.33μm for a tilt incident angle of 6°. For a pixel with a size of *P*, the ratio of the light which transmits through adjacent pixels can be expressed with *W*/*P*. If the ratio equals to zero, it illustrates that the light is the vertical incidence and that it goes through just one pixel. For an incident angle of 6°, the ratio is only 1.77% and it may be ignored. As such, the LCWFC may be used at the tilt incidence condition with a little tilt angle.

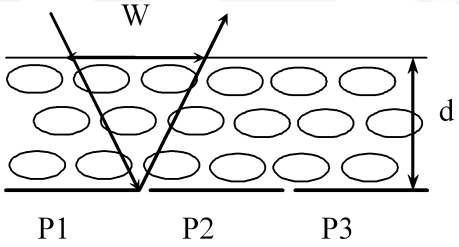

Figure 16. Illustration of the pixel crossover - P1, P2 and P2 are pixels, *d* is the thickness of the cell.

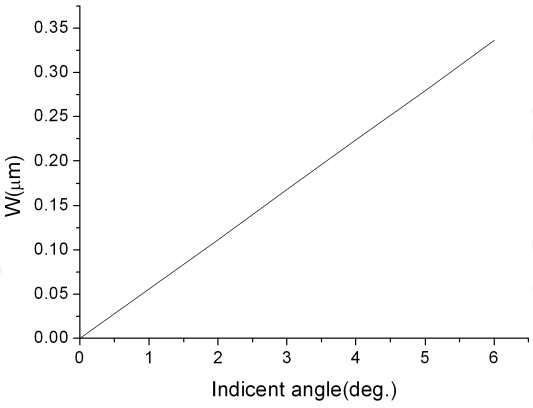

Figure 17. The pixel crossover *W* as a function of the incident angle.

2.9. Diffraction efficiency with tilt incidence

Because the phase of each pixel changes with the tilt incidence, the diffraction efficiency will decrease [64]. The Fresnel phase lens model [71] is used to calculate the change of the diffraction efficiency and 16 quantified levels are selected. The simulated results show that at an incident angle of 6°, the diffraction efficiency is reduced by 3% (Fig.18). For the incident angles less than 3°, the reduction in diffraction efficiency is less than 1% - a negligible loss for most applications.

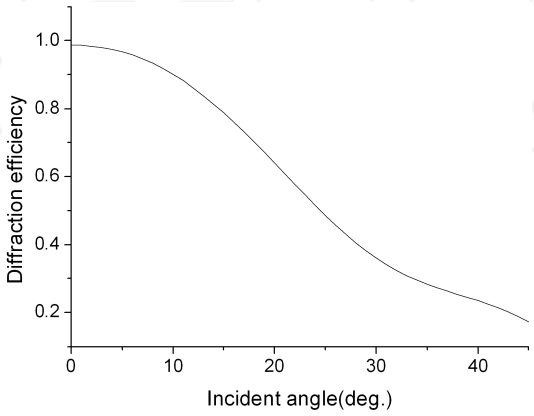

Figure 18. Diffraction efficiency as a function of the incident angle.

2.9.1. Chromatism

The chromatism of the LCWFC includes refractive index chromatism and quantization chromatism. Refractive index chromatism is caused by the LC material, and is generally called dispersion. Meanwhile, quantization chromatism is caused by the modulo 2π of the phase wrapping. Theoretically, the LCWFC is only suitable for use in wavefront correction for a single wavelength and not on a waveband due to chromatism. However, if a minor error is allowed, LCWFC can be used to correct distortion within a narrow spectral range.

2.10. Effects of chromatism on the diffraction efficiency of LCWFC

The measured birefringence dispersion of a nematic LC material (RDP-92975, DIC) is shown in Fig. 19. It can be seen that the birefringence Δn is dependent on the wavelength and the dispersion of the LC material is particularly severe when the wavelength is less than 500 nm. Since a phase wrapping technique is used, the phase distribution should be modulo 2π, and it should then be quantized [71]. Assuming that the quantization wavelength is λ_0, the thickness of the LC layer is d, and V_{max} denotes the voltage needed to obtain a 2π phase modulation, such that the maximum phase modulation of the LCWFC can be expressed as:

$$\Delta\varphi_{\max}(\lambda_0) = 2\pi \frac{\Delta n(\lambda_0, V_{\max})d}{\lambda_0} = 2\pi \tag{20}$$

For any other wavelength λ, it can be rewritten as:

$$\Delta\varphi_{\max}(\lambda) = 2\pi \frac{\Delta n(\lambda, V_{\max})d}{\lambda} \tag{21}$$

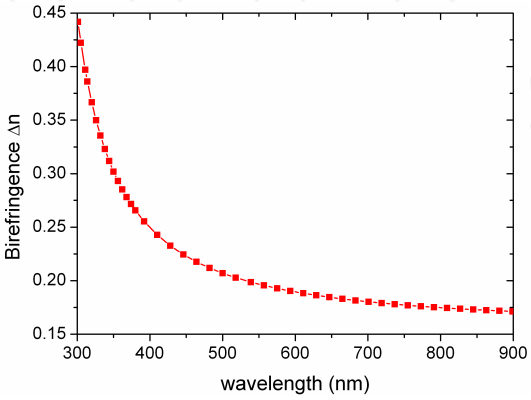

Figure 19. The birefringence *Δn* as a function of the wavelength.

For a quantization wavelength of 550 nm, 633 nm and 750 nm, the variation of the maximum phase modulation as a function of wavelength is shown in Fig. 20. Assuming that the deviation of the phase modulation is 0.1, for λ_0=550, 633 and 750 nm, the corresponding spectral ranges are calculated as 520–590 nm, 590–690 nm and 690–810 nm, respectively. If a 10% phase modulation error is acceptable, then the LCWFC can only be used to correct the distortion for a finite spectral range.

The variation of Δn and λ affects the diffraction efficiency of the LCWFC. Using the Fresnel phase lens model, the diffraction efficiency for any other wavelength λ can be described as [80]:

$$\eta = \left| \frac{\sin(\pi d\Delta n(\lambda, V_{\max}) / \lambda)}{\pi(d\Delta n(\lambda, V_{\max}) / \lambda - 1)} \right|^2 \tag{22}$$

The effects of Δn and λ on the diffraction efficiency are shown in Fig. 21. For λ_0 = 550 nm, 633 nm and 750 nm, and their respective corresponding wavebands of 520–590 nm, 590–690 nm and 690–810 nm, the maximum energy loss is 3%, which is acceptable for

the LC AOS. Although only one kind of LC material is measured and analysed, the results are helpful in the use of LCWFCs because almost all the nematic LC materials have similar dispersion characteristics.

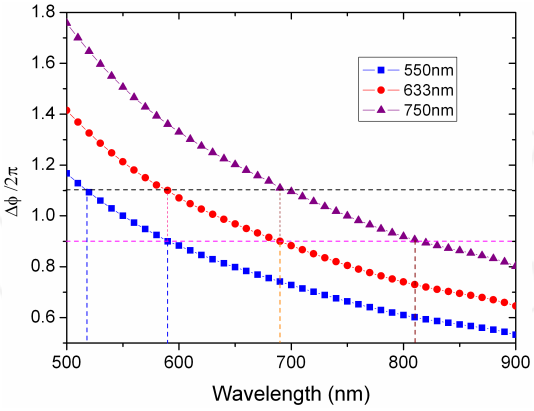

Figure 20. The phase modulation as a function of the wavelength for λ_0 = 550 nm, 633 nm and 750 nm, respectively - the two horizontal dashed lines indicate the phase deviation range while the four vertical dashed lines illustrate three sub-wavebands of 520–590 nm, 590–690 nm and 690–820 nm, respectively.

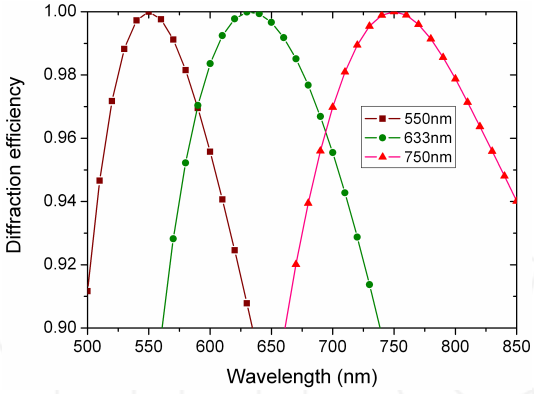

Figure 21. The diffraction efficiency as a function of wavelength for λ_0 = 550 nm, 633 nm and 750 nm, respectively.

2.11. Broadband correction with multi-LCWFCs

The above calculated results show that it is only possible to correct the distortion in a narrow waveband using only one LCWFC. Therefore, to realize the distortion correction in a broadband - such as 520–810 nm - multi-LCWFCs are necessary; each LCWFC is responsible for the correction of different wavebands and then the corrected beams are combined to re-

alize the correction in the whole waveband. The proposed optical set-up is shown in Fig. 22, where a polarized beam splitter (PBS) is used to split the unpolarized light into two linear polarized beams. An unpolarized light can be looked upon as two beams with cross polarized states. Because the LCWFC can only correct linear polarized light, an unpolarized incident light can only be corrected in one polarization direction while the other polarized beam will not be corrected. Therefore, if a PBS is placed following the LCWFC, the light will be split into two linear polarized beams: one corrected beam goes to a camera; the other uncorrected beam is used to measure the distorted wavefront by using a wavefront sensor (WFS). This optical set-up looks like a closed loop AOS, but it is actually an open-loop optical layout. This LC adaptive optics system must be controlled through the open-loop method [31, 81]. Three dichroic beam splitters (DBSs) are used to acquire different wavebands. A 520–810 nm waveband is acquired by using a band-pass filter (DBS1). This broadband beam is then divided into two beams by a long-wave pass filter (DBS2). Since DBS2 has a cut-off point of 590 nm, the reflected and transmitted beams of the DBS2 have wavebands of 520–590 nm and 590–820 nm, respectively. The transmitted beam is then split once more by another long-wave pass filter (DBS3) whose cut-off point is 690 nm. Through DBS3, the reflected and transmitted beams acquire wavebands of 590–690 nm and 690–810 nm, respectively. Thus, the broadband beam of 520–810 nm is divided into three sub-wavebands, each of which can be corrected by an LCWFC. After the correction, three beams are reflected back and received by a camera as a combined beam. Using this method, the light with a waveband of 520–810 nm can be corrected in the whole spectral range with multi-LCWFCs.

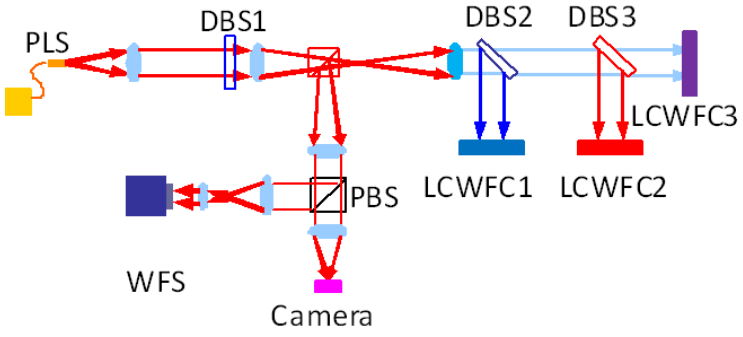

Figure 22. Optical set-up for a broadband correction - PLS represents a point light source, PBS is a polarized beam splitter, DBS means dichroic beam splitter, DBS1 is a band-pass filter, and DBS2 and DBS3 are long-pass filters.

The broadband correction experimental results are shown in Fig. 23. A US Air Force (USAF) resolution target is utilized to evaluate the correction effects in a broad waveband. Firstly, the waveband of 520–590 nm is selected to perform the adaptive correction. After the correction, the second element of the fifth group of the USAF target is resolved, with a resolution of 27.9 μm (Fig.23(b)). Considering that the entrance pupil of the optical set-up is 7.7 mm, the diffraction-limited resolution is 26.4 μm for a wavelength of 550 nm. Thus, a near dif-

fraction-limited resolution has been achieved. Figure 23(c) shows the resolving ability for a waveband of 590–690 nm. The first element of the fifth group is resolved and the resolution is 31.25 μm, which is near the diffraction-limited resolution of 30.4 μm for a 633 nm wavelength. The corrected result for 520–690 nm is shown in Fig. 23(d). The first element of the fifth group can also be resolved. These results show that a near diffraction-limited resolution of an optical system can be obtained by using multi-LCWFCs.

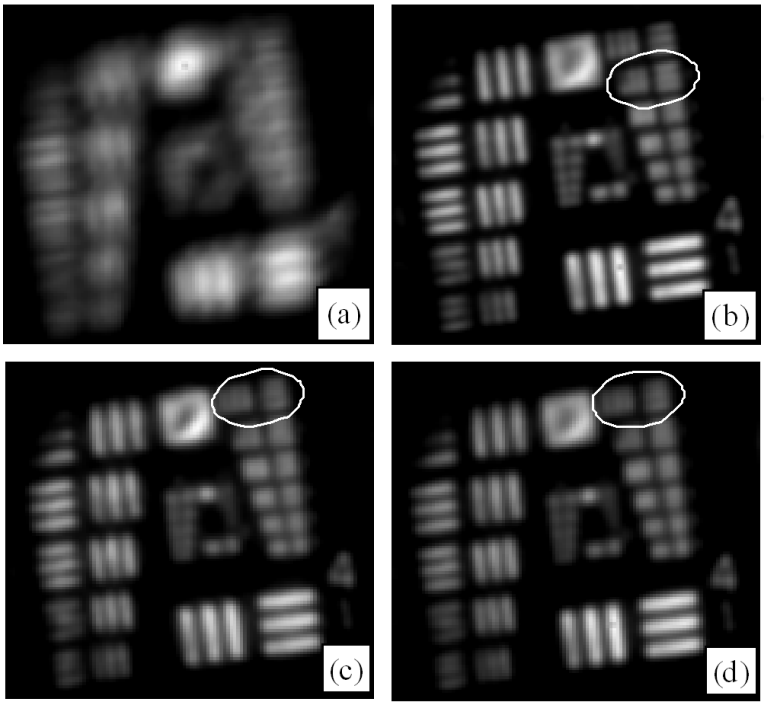

Figure 23. Images of the resolution target for different wavebands: (a) no correction; (b) 520–590 nm; (c) 590–690 nm; (d) 520–690 nm - the circular area represent the resolving limitation.

2.11.1. Fast response liquid crystal material

In applications of LCWFCs, the response speed is a key parameter. A slow response will significantly decrease the bandwidth of LC AOS. To improve the response speed, dual-frequency and ferroelectric LCs have been utilized to fabricate the LCWFC [82, 83]. However, there are some shortcomings with these fast materials. The driving voltage of the dual-frequency LCWFC is high and it is incompatible with the very large scale integrated circuit. The phase modulation of the ferroelectric LCWFC is very slight and it is hard to correct the distortions. Nematic LCs have no such problems. However, its response speed is slow. In this section, we introduce how to improve the response speed of nematic LCs.

For a nematic LC device, the response time of LC can be described by the following equations when the LC cell is in parallel-aligned mode [84]:

$$\tau_{rise} = \frac{\gamma_1 d^2}{K_{11}\pi^2 \quad \left(V / V_{th}\right)^2 - 1} \tag{23}$$

$$\tau_{decay} = \frac{\gamma_1 d^2}{K_{11}\pi^2} \tag{24}$$

where γ_1 is the rotational viscosity, V and V_{th} are turn-on driving and threshold voltage, K_{11} is the elastic constant and d is the thickness of the LC cell. Generally, the rise time can be decreased by the overdriving method. However the decay time particularly depends upon the intrinsic parameters of LC devices, which are the key factors for response improvement. From Eq. (24), the smaller visco-elastic coefficient (γ_1/K_{11}) and d is, the shorter the response time is. However, it is necessary to keep the phase retardation ($d\times\Delta n$) to exceed (or equal) one wavelength for a LCWFC, and then the cell gap can only been reduced to a limited value for a constant birefringence (Δn). The higher birefringence of LC materials enables a thinner cell gap to be used while keeping the same phase retardation and improves the response performance of the LCWFC. Therefore, the LC materials with high Δn and low γ_1/K_{11} are required to have a fast response.

In the study of fast response LC materials, a concept of 'figure-of-merit' (*FoM*) is adopted to evaluate different LC compounds [85], as shown as Eq. (25). A LC material with a high *FoM* value will provide a short response time:

$$FoM = K_{11}\Delta n^2 / \ \gamma_1 \tag{25}$$

2.12. Nematic liquid crystal molecular design

In practice, some simple empirical rules together with a trial are usually used to help with the molecular design and mixing, such as LC compounds with a tolane and biphenyl group with a large Δn and a moderate γ_1. Recently, some computer simulation-based theoretical studies have been performed in order to shed light on the connections between macroscopic properties and molecular structure. A notable advantage of simulation is to predict the properties of a nematic LC material with optimal molecular configurations instead of costly and time-consuming experimental synthesis. In the study of fast response LCs, theoretical methods are used to analyse the rotational viscosity and Δn of a specific chemical structure.

In the study of the rotational viscosity (RVC) of nematic liquid crystals, Zhang et al. [86] adopt two statistical-mechanical approaches proposed by Nemtsov-Zakharov (NZ) [87] and Fialkowski (F) [88]. The NZ approach is based on the random walk theory. It is a correction

of its predecessor in considering the additional correlation of the stress tensors with the director and the fluxes with the order parameter tensor, except for the autocorrelation of the microscopic stress tensor.

In Fig.24, the RVC of the nematic liquid crystal E7 is shown as a function of temperature. The experimental rotational viscosity decreases with temperature, and similar variations from NZ and F's theoretical methods are also obtained. The calculated NZ and F rotational viscosities are in the same order of magnitude as the experimental values. The larger the number of molecules, the longer the simulation time, and the revised force field for liquid crystals is expected to be helpful in improving this prediction.

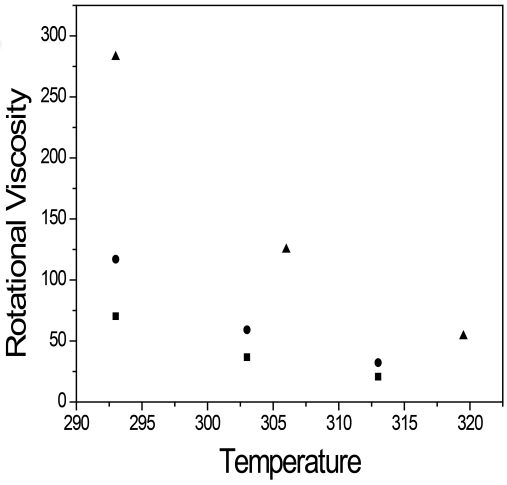

Figure 24. Temperature dependence of the rotational viscosity for E7, ■, the NZ method, ●, the F method, ▲, and the experiment.

The birefringence and dielectric anisotropy can be calculated by the Vuks equation and the Maier-Meier theory, respectively, and these calculated values have a good correlation with the experimental data in Ref. 89. In all, these approaches comprise a unique molecular design method for fast response LCs.

2.13. Chemosynthesis of fast response LC materials

In order to achieve fast LC material, researchers have synthesized a series of high birefringence LC materials with a linear shape and a long conjugated group. Gauza et al. first synthesized and reported a biphenyl, cyclohexyl- biphenyl isothiocyanato (NCS) LC material in which Δn is 0.2-0.4 and the rotational viscosity is about 10 ms μm^{-2}. The chemical structures are shown in Fig. 25. Moreover, they perform a comparison with a commercial E7 mixture. At 70°C, the *FoM* of the NCS mixture has a factor ten higher than that of E7 at 48°C [90].

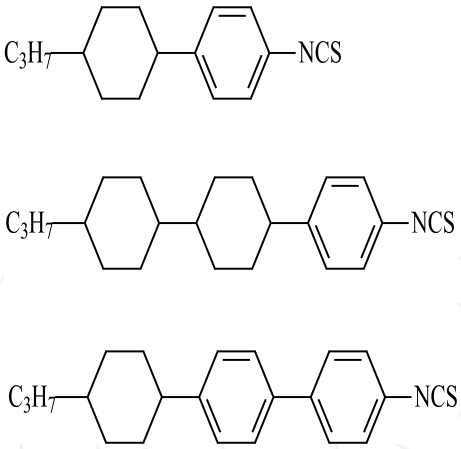

Figure 25. Chemical structures of biphenyl, cyclohexyl- biphenyl isothiocyanato LC materials.

In 2006, Gauza [91] provided one type of NCS LC material with unsaturated groups. The LC chemical structures are shown in Fig. 26: the final two NCS LC mixtures show a Δn value of 0.25 and 0.35; a viscosity factor of about 6 ms μm^{-2}; *FoM* values of 10.1 and 18.7 $\mu m^2\ s^{-1}$. The response speed of such a LC material can be as low as 640 μs with a LC thickness of 2 μm at 35°C.

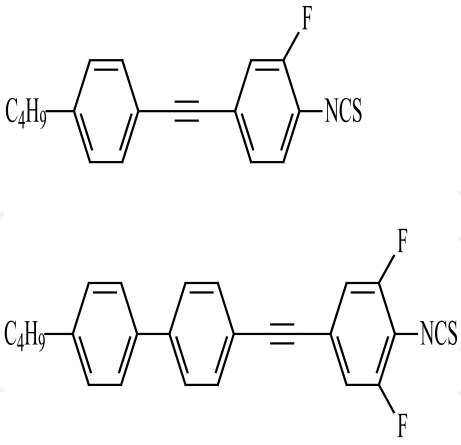

Figure 26. Chemical structures of NCS LC materials with unsaturated groups.

The high birefringence isothiocyanato LC with a tolane or terphenyl group can usually be synthesized via a couple reaction; the chemical reaction route was shown in Fig. 27 [92]:

http://dx.doi.org/10.5772/54265

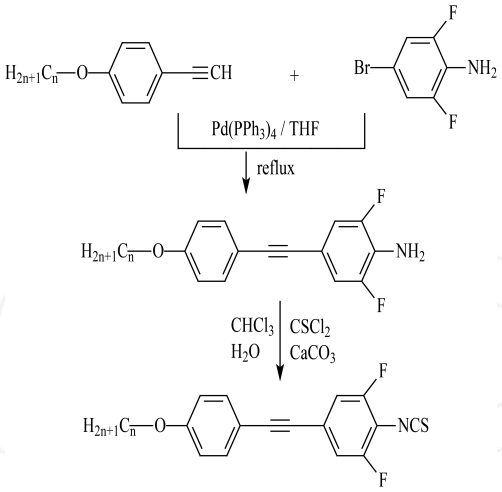

Figure 27. The synthesis of isothiocyanato compounds using Suzuki coupling.

In Gauza et al., in subsequent research, a series of fluro-substituted NCS LC materials with a Δn up to 0.5 at room temperature was developed, and some of them show better response performance [93], the chemical structures are shown in Fig. 28:

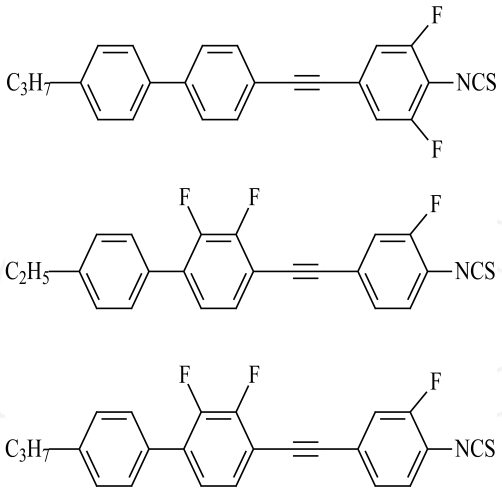

Figure 28. Chemical structures of NCS LC materials with high birefringence.

In the research of isothiocyanate tolane LC compounds, Peng et al. prepared a NCS LC compound via an electronation reaction. The reaction route is shown in Fig. 29. Com-

pared to the conventional couple reaction method, this synthesis route improves the total reaction yield [94].

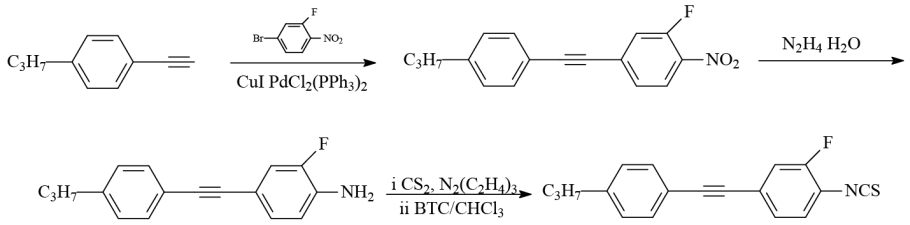

Figure 29. The synthesis of isothiocyanato tolane LC compound using electronation reaction.

It has rarely been reported that LCs with a very low rotational viscosity were mixed to high Δn LCs in order to improve response performance. However, Peng et al. introduce a type of difluorooxymethylene-bridged (CF_2O) LCs with a very low rotational viscosity so as to improve the response performance of NCS LCs. The chemical structure is shown in Fig. 30. When the material was mixed to NCS LCs with a high Δn, the visco-elastic coefficient of mixture decreased noticeably, the LC mixture approximately maintained high birefringence, and the *FoM* value increased from 14.8 to 16.9 $\mu m^2 s^{-1}$ at 7% concentration [95].

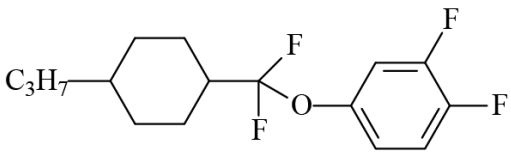

Figure 30. Chemical structure of difluorooxymethylene- bridged LC compound.

Acknowledgements

This work is supported by the National Natural Science Foundation of China, with Grant Nos. 50703039, 60736042, 11174274 and 11174279.

Author details

Li Xuan, Zhaoliang Cao, Quanquan Mu, Lifa Hu and Zenghui Peng

State Key Laboratory of Applied Optics, Changchun Institute of Optics, Fine Mechanics and Physics, Chinese Academy of Sciences, Jilin Changchun, China

http://dx.doi.org/10.5772/54265

References

[1] F. Reinitzer, Monatsh. Chemie, 9, 421–425 (1888).

[2] D. Dayton, S. Browne, J. Gonglewski. SPIE, 5894, 58940M.1-58940M.6 (2005).

[3] D. C. Dayton, S. L. Browne, J. D. Gonglewski, S. R. Restaino. Appl. Opt., 40, 2345-2355 (2001).

[4] J. Amako, T. Sonehara. Applied Optics, 30, 4622-4628 (1991).

[5] M. T. Gruneisen, L. F. DeSandre, J. R. Rotge, R. C. Dymale, D. L. Lubin. Opt. Eng., 43, 1387-1393 (2004).

[6] M. T. Gruneisen, R. C. Dymale, M. B. Garvin. SPIE, 5894, 589412.1-589412.10 (2005).

[7] M. T. Gruneisen, L. F. Desandre, J. R. Rotge, R. C. Dymale, D. L. Lubin. Opt. Eng., 43, 1387-1393 (2004).

[8] M. T. Gruneisen, R. C. Dymale, J. R. Rotge, L. F. Desandre, D. L. Lubin. Opt. Eng., 44, 023201.1-023201.9 (2005).

[9] I. N. Kompanets, Zarubezh. Radioelektron, 4, 46 (1977).

[10] S. T. Kowel, D. S. Cleverly. "A Liquid Crystal Adaptive Lens," in Proceedings, NASA Conference on Optical Information Processing for Aerospace Applications, Hampton, Va. (1981).

[11] S. T. Kowel, P. Kornreich, A. Nouhi. “Adaptive spherical lens,” Applied Optics, Vol. 23, No. 16, 2774-2777 (1984).

[12] A. A. Vasil’ev, A. F. Naumov, V. I. Shmal’gauzen. Sov. J. Quantum Electron., 16, 471-474 (1986).

[13] A. Vasil’ev, M. A. Vorontsov, A. V. Koryabin, A. F. Naumov, V. I. Shmal’gauzen. Sov. J. Quantum Electron. 19, 395-398 (1989).

[14] D. Bonaccini, G. Brusa, S. Esposito, P. Salinari, P. Stefanini. SPIE, 1334, 89-97 (1990).

[15] D. Bonaccini, G. Brusa, S. Esposito, P. Salinari, P. Stefanini, V. Biliotti. SPIE, 1543, 133-143 (1991).

[16] R. Dou, M. K. Giles. Optics Letters, 20, 1583-1585 (1995).

[17] S. R. Restaino. SPIE, 2200, 46-48 (1994).

[18] S. R. Restaino, T. Martinez, J. R. Andrews, S. W. Teare. SPIE, 4825, 41-45 (2002).

[19] P. V. Mitchell. “Innovative adaptive optics using liquid crystal light valve,” Optical Society of America, (1992).

[20] G. D. Love, J. S. Fender, S. R. Restaino. Opt. And Phot. News, 6, 16-20 (1995).

[21] G. D. Love, John V. Major, Alan Purvis. Optics Letters, 19, 1170-1172 (1994).

[22] A.V. Kudryashov, J. Gonglewski, S. Browne, R. Highland. Opt. Comm. 141, 247-253 (1997).

[23] D. C. Dayton, S. L. Browne, S. P. Sandven, J. D. Gonglewski, and A. V. Kudryashov. App. Opt., 37, 5579-5589 (1998).

[24] T. L. Kelly, G. D. Love. App. Opt., 38, 1986-1989 (1999).

[25] G. T. Bold, T. H. Barnes, J. Gourlay, R. M. Sharples, T. G. Haskell. Optics Communications, 148, 323-330 (1998).

[26] J. Gourlay, G. D. Love, P. M. Birch, R. M. Sharples, and A. Purvis. Opt. Comm., 137, 17-21 (1997).

[27] D. Bonaccini, et. al. SPIE, 2000, 96-98 (1993).

[28] V. A. Dorezyuk, A. F. Naumov, V. I. Shmalgauzen. Sov. Phys. Tech. Phys., 34, 1384 (1989).

[29] W. Klaus, et. al. SPIE, 3635, 66-73 (1999).

[30] D. Dayton, J. Gonglewski, S. Restaino, J. Martin, J. Phillips, M. Hartman, S. Browne, P. Kervin, J. Snodgrass, N. Heimann, M. Shilko, R. Pohle, B. Carrion, C. Smith, D. Thiel. Optics Express, 10, 1508-1519 (2002).

[31] Quanquan Mu, Zhaoliang Cao, Lifa Hu, Yonggang Liu, Zenghui Peng, Lishuang Yao, Li Xuan. Optics Communications, 285, 896-899 (2012)

[32] Zenghui Peng, Yonggang Liu, Lishuang Yao, Zhaoliang Cao, Quanquan Mu, Lifa Hu, and Li Xuan. Optics Letters, 36, 3608–3610 (2011).

[33] Quanquan Mu, Zhaoliang Cao, Lifa Hu, Yonggang Liu, Zenghui Peng, Li Xuan. Optics Express, 18, 21687-21696 (2010)

[34] Zhaoliang Cao, Quanquan Mu, Lifa Hu, Yonggang Liu, Li Xuan. Optics Communications, 283,946-950 (2010)

[35] Zhaoliang Cao, Quanquan Mu, Lifa Hu, Xinghai Lu, and Li Xuan. Opt. Express, 17, 9330-9336 (2009).

[36] Zhaoliang Cao, Quanquan Mu, Lifa Hu, Dayu Li, Zenghui Peng, Yonggang Liu, Li Xuan. Opt. Express, 17, 2530-2537 (2009).

[37] Ran Zhang, Jun He, Zenghui Peng, Xuan Li. Chinese Physics B, 18, 2885-92 (2009).

[38] Zhaoliang Cao, Quanquan Mu, Lifa Hu, Dayu Li, Yonggang Liu, Lu Jin, Li Xuan. Opt. Express, 16, 7006-7013 (2008)

[39] Zhaoliang Cao, Quanquan Mu, Lifa Hu, Yonggang Liu, Zenghui Peng, Li Xuan. Applied Optics, 47, 1785-1789 (2008)

[40] Quanquan Mu, ZhaoLiang Cao, Dayu Li, Lifa Hu, Li Xuan. Applied Optics, 47, 4297-4301 (2008).

[41] Zhaoliang Cao, Li Xuan, Lifa Hu, Yongjun Liu, Quanquan Mu, Dayu Li. Optics Express, 13, 1059-1065 (2005).

[42] Lifa Hu, Li Xuan, Yongjun Liu, Zhaogliang Cao, Dayu Li, QuanQuan Mu. Optics Express, 12, 6403-6409 (2004).

[43] F. V. Martin, P. M. Prieto, P. Artal. J. Opt. Soc. Am. A, 15, 2552-2562 (1998).

[44] A. Awwal, B. Bauman, D. Gavel, S. S. Olivier, S. Jones, J. L. Hardy, T. Barnes, J. S. Werner. SPIE, 5169, 104-122 (2003).

[45] W. Quan, Z. Wang, G. Mu, L. Ning. Optik, 114, 1-5 (2003).

[46] X. Wang, D. Wilson, R. Muller, P. Maker, D. Psaltis. Applied Optics, 39, 6545-6555 (2000).

[47] S. Serati, J. Stockley. IEEE Aerospace Conf. Proc. 3, 1395-1402, (2002).

[48] J. Stockley, S. Serati. SPIE, 5550, 32-39 (2004).

[49] N. V. Tabiryan, S. R. Nersisyan. Applied Physics Letters, 84, 5145-5147 (2004).

[50] S. Serati, J. Stockley. SPIE, 5894, 58940K.1-58940K.13 (2005).

[51] M. Reicherter, T. Haist, E. U. Wagemann, H. J. Tiziani. Optics Letters, 24, 608-610 (1999).

[52] W. Hossack, E. Theofanidou, J. Crain, K. Heggarty, M. Birch. Optics Express, 11, 2053-2059 (2003).

[53] L. Quesada, J. Andilla, E. M. Badosa. Applied Optics, 48, 1084-1090 (2009).

[54] S. Krueger, G. Wernicke, H. Gruber, N. Demoli, M. Duerr, S. Teiwes. SPIE, 4294, 84-91 (2001).

[55] G. Wernicke, S. Kruger, H. Gruber, N. Demoli, M. Durr, S. Teiwes. SPIE, 4596, 182-190 (2001).

[56] P. Ambs, L. Bigue, E. Hueber. SPIE, 5518, 92-103 (2004).

[57] I. Moreno, A. Marquez, J. Nicolas, J. Campos, M. J. Yzuel. SPIE, 5456, 186-196 (2004).

[58] V. G. Chigrinov. SPIE, 5003, 130-137 (2003).

[59] L. Scolari, T. T. Alkeskjold, J. Riishede, A. Bjarklev, D. S. Hermann, Anawati, M. D. Nielsen, P. Bassi. Optics Express, 13, 7483-7496 (2005).

[60] J. D. Schmidt, M. E. Goda, B. D. Duncan. SPIE, 6711, 67110M.1-67110M.12 (2007).

[61] L. Hu, L. Xuan, Z. Cao, Q. Mu, D. Li, Y. Liu. Optics Express, 14, 11911-11918 (2006).

[62] K. Hirabayashi, T. Yamamoto, M. Yamaguchi. “Free space optical interconnections with liquid crystal microprism arrays,” Applied Optics, Vol. 34, 2571-2580 (1995).

[63] Y. H. Lin, M. Mahajan, D. Taber, B. Wen, B. Winker. SPIE, 5892, 58920C.1-58920C.10 (2005).

[64] M. Ferstl, B. Kuhlow, E. Pawlowski. Optical Engineering, 33 1229-1235 (1994).

[65] H. Li, Z. Lu, J. Liao, Z. Weng. Acta Photonica Sinica, 29, 559-563 (2000) (In Chinese).

[66] P. Xu, X. Zhang, L. Guo, Y. Guo, et al. Acta Photonica Sinica, 16, 833-838 (1996) (In Chinese).

[67] R. Hudgin. J. Opt. Am., 67, 393-395 (1977).

[68] F. Roddier, Adaptive Optics in Astronomy (Cambridge University Press, 1999), pp. 13-15.

[69] R. K. Tyson, Principles of adaptive optics (Second Edition Academic Press 1997), pp. 71.

[70] G. D. Love, "Liquid crystal adaptive optics," in: Adaptive optics engineering handbook (R. K. Tyson, CRC, 1999).

[71] Z. Cao, L. Xuan, L. Hu, Y. Liu, Q. Mu. Opt. Express 13, 5186-5191 (2005).

[72] L. N. Thibos, A. Bradley. Optometry and Vision Science 74, 581-587 (1997).

[73] Z. Cao, Q. Mu, L. Hu, et al. Chin. Phys., 16, 1665-1671 (2007).

[74] R. J. Noll. J. Opt. Soc. Am., 66, 207-211 (1976).

[75] N. Roddier. Optical Engineering, 29, 1174-1180 (1990).

[76] Mikhail Loktev, Gleb Vdovin, Nikolai Klimov, et al. Opt. Express, 15, 2770-2778 (2007).

[77] U. Efron, J. Grinberg, P. O. Braatz, M. J. Little, P. G. Reif, R. N. Schwartz. J. Appl. Phys., 57, 1356-1368 (1985).

[78] U. Efron, S. T. Wu, J. Grinberg, L. D. Hess. Opt. Eng., 24, 111-118 (1985).

[79] N. Konforti, E. Marom, S. T. Wu. Optics Letters, 13, 251-253 (1988).

[80] V. Laude. Optics Communications, 153, 134-152 (1998).

[81] Quanquan Mu, ZhaoLiang Cao, Dayu Li, Lifa Hu, Li Xuan. Applied Optics, 47, 4297-4301 (2008).

[82] Gu, B. Winker, B. Wen, et al. Proc. SPIE, 5553, 68-82, (2004).

[83] P. Birch, J. Gourlay, G. Love, et al. Appl. Opt., 37, 2164-2169 (1998).

[84] Jakeman, E.P. Raynes Phys. Lett., 39A, 69-70 (1972).

[85] S. Gauza, H. Wang, C. Wen, S. Wu, A. Seed, R. Dabrowski, Jpn. J. Appl. Phys., 42, 3463-3466 (2004).

[86] R. Zhang, Z. Peng, Y. Liu, L. Xuan. Chinese Physics B, 18, 4380-4385 (2009).

[87] A.V. Zakharov, A. V. Komolkin, A. Maliniak. Phys. Rev. E, 59, 6802-6807 (1999).

[88] M. Fialkowski Phys. Rev. E, 58, 1955-1966 (1998).

[89] M. F. Vuks, Opt & Spectroscopy, 20, 361-368 (1966).

[90] S. Gauza, H. Wang, C. Wen, S. Wu, A. Seed, R. Dabrowski. Jpn. J. Appl. Phys., 42, 3463-3466 (2004).

[91] S. Gauza, C. Wen, B. Wu, S. Wu, A. Spadlo, R. Dabrowski. Liq. Cryst., 33, 705-710 (2006).

[92] C. O. Catanescu, S. T. Wu, L. C. Chien. Liq. Cryst., 31, 541-555 (2004).

[93] S. Gauza, A. Parish, S. Wu, A. Spadlo, R. Dabrowski. Liq. Cryst., 35, 483-488 (2008).

[94] Z. Peng, Y. Liu, L. Yao, et al. Chinese Journal of Liquid Crystal and Display, 26, 427-431 (2011) (In Chinese).

[95] Z. Peng, Y. Liu, L. Yao, Z. Cao, Q. Mu, L. Hu, X. Lu, L. Xuan, Z. Zhang. Chinese Physics Letters, 28, 094207-1-094207-3 (2011).

INTECH